ARTICLE NO. 78-977R

Aerothermochemical Analysis of Erosive Burning in a Laboratory Solid-Rocket Motor

Robert A. Beddini*
Aeronautical Research Associates of Princeton, Inc., Princeton, N.J.

An analysis of steady-state combustion and flow phenomena in a two-dimensional, laboratory-type solid-propellant motor is presented with emphasis on the condition of erosive burning. The problem is treated as a confined, reacting turbulent shear-flow using a second-order turbulence closure model. Low Reynolds number and propellant surface roughness effects are accounted for. Comparison of calculated results with cold flow experimental data confirms that development of the mean velocity profile is initially well described by laminar, "inviscid" theory. However, due to the rapid development of turbulence within the simulated grain-port, transition to a turbulent velocity profile is predicted to occur at center port Reynolds numbers greater than those obtained in the considered experiments. Transition of the velocity profile is theoretically found to occur prior to the onset of erosive burning in real motor environments. Comparisons of calculated results with measured static pressure distributions have been made for a composite-propellant "slab" motor. Good agreement with static pressure data is obtained for propellant roughness heights which are approximately 10% of the larger AP crystal diameters, with surface roughness significantly affecting erosive burning. Theoretical comparison with the Lenoir-Robillard model also indicates that the present model predicts a much more rapid decrease in erosive burning as the port hydraulic radius is increased.

Nomenclature

A = Arrhenius pre-exponential coefficient
a,b = turbulence modeling parameters (3.25, 0.125)
B_g = effective reaction rate coefficient
c_p = specific heat at constant pressure
c_π = specific heat of propellant
D = overall diffusion coefficient
g_{lm} = metric tensor, $\partial x_l/\partial x_m$
h = specific sensible enthalpy, c_pT
h_α^0 = heat of formation at 0 K
H = total enthalpy, $H=h+u^iu_i/2$
k = thermal conductivity
k_s = equivalent sand roughness height
L_s^0 = heat of decomposition at 0 K
$\dot{m}_s$ = surface mass flux
n = normal burning rate pressure exponent
n_j = surface normal vector
p = static pressure
p^* = reference pressure, 6.9×10^7 dyne/cm^2 (1000 psi)
q = rms intensity, $(\overline{u'^iu'_i})^{1/2}$
$\dot{r}$ = regression (burning) rate, $\dot{m}_s/\rho_\pi$
$\dot{r}_n$ = normal (nonerosive) regression rate
R = gas constant per unit mole
Re_c = Reynolds number, $\bar{\rho}_c\bar{u}_c\delta/\bar{\mu}_c$
Re_s = Reynolds number, $\bar{\rho}_s\bar{v}_s\delta/\bar{\mu}_s$
t = time
T = static temperature
T_A = activation temperature (energy/R)
T_i = interior propellant temperature
u_j = velocity vector $\{u,v,w\}$
W_α = molecular weight of species α
x_j = coordinate vector $\{x,y,z\}$
Y_α = mass fraction
β = temperature exponent of reaction pre-exponential coefficient
δ = half-height of port
Δh_g = heat of reaction per unit mass
Λ = turbulent macrolength scale
μ = viscosity
ω = specific reaction source term
ρ = density
Φ = concentration (pressure) exponent in reaction rate

Superscripts

$\bar{(\ )}$ = time average of variable
$(\ )'$ = turbulent fluctuating value of variable

Subscripts

c = centerline
e = reaction end state
g = gas phase
h = condition at port head end
s = condition at surface
α = index for chemical species
π = denotes propellant solid phase
$(\ ,\ )$ = differentiation
$*$ = reaction initial state

Presented as Paper 78-977 at the AIAA/SAE 14th Joint Propulsion Conference, July 25-27, 1978; submitted Aug. 25, 1978; revision received Jan. 16, 1980.

Index categories: Solid and Hybrid Rocket Engines; Reactive Flows; Boundary Layers and Convective Heat Transfer—Turbulent.

*Consultant, currently, Senior Research Scientist, Princeton Combustion Research Laboratories, Inc., Princeton, N.J. Member AIAA.

Introduction

CONTEMPORARY solid-propellant rocket motors often utilize a central port—the "grain port"—through which the combustion gases flow. An assumption which is almost universally used in analyses of motor performance is that the flow properties within the grain port may be represented by their bulk averages over a cross section. This assumption is practical and adequate providing closure relationships are available for describing inherently multidimensional processes occurring near the port surface (e.g., combustion and viscous friction). The closure process becomes more formidable when propellant combustion locally interacts with the fluid dynamics. One such interaction effect, which can lead to a substantial increase in the mean propellant burning

rate under high port velocity conditions, is termed erosive burning.

Reviews of erosive burning theoretical treatments and experimental investigations may be found in Williams et al.,[1] Kuo and Razdan,[2] and in the analysis of Mukunda,[3] King,[4] Beddini,[5] and Razdan and Kuo.[6] These analyses all assume that the flow within the grain port of a solid-rocket motor is of classical boundary-layer type. Specifically, velocity profile solutions for a turbulent boundary layer are developed (with various levels of analytic and empirical approximation) subject to matching to a uniform "core" flow which is assumed to exist within the central region of the port. The gradient of the velocity profile enters into the specification of turbulent diffusivity in the propellant flame zone, which in turn governs the magnitude and scaling of erosive burning.

To experimentally simulate the flowfield in the grain port of actual rocket motors, Dunlap et al.[7] and Yamada et al.[8] have investigated the flow in a porous tube and channel, respectively, with transpiration through the side wall. The Reynolds numbers (based on transpiration velocity and characteristic diameter) of these experiments were within the range associated with typical rocket motors. Based on the experimental results, both of these investigations concluded that the mean velocity profiles in actual rocket motors corresponded with self-similar solutions to the laminar Navier-Stokes equations in the inviscid limit. No evidence of a uniform core flow region was found, since the mean velocity profiles were similar in some respects to those in laminar pipe or channel flow. In addition, appreciable levels of turbulence were found, and Yamada et al. showed that the turbulence intensity profile behaved in a substantially different manner from typical turbulent channel flow. These experimental investigations have therefore posed some serious questions concerning the nature of the flowfield in actual motors, and for the assumptions used in erosive burning analyses. The mean flow behavior has also been shown by Culick[9] to affect the aeroacoustics of the solid rocket motor.

The principal objective of the present investigation is to analyze the flowfield in the solid-rocket motor and its effects on erosive burning. It will be shown that the conflicting cold flow experimental results and prior analytical assumptions concerning the turbulent velocity profile can be substantially reconciled. In addition, the effects of propellant surface roughness and motor size on erosive burning will also be investigated. The problem is approached by extending the reacting turbulent boundary-layer analysis developed in Ref. 5. This approach utilizes a semiempirical, second-order closure description of turbulence and is sufficiently comprehensive to account for several aerothermochemical features of interest. The general model developed herein will be referred to as the solid-propellant erosive combustion (SPEC) model in the text.

Table 1 Major assumptions

1) Single-step, homogeneous, and stoichiometric gas phase reaction.
2) Specific heats of species are equal and independent of temperature.
3) $k/c_p = \rho D = \mu(T)$ (Prandtl and Lewis numbers of unity).
4) Surface decomposition of a homogeneous propellant is governed by Arrhenius kinetics.
5) Turbulent correlations involving the temporal pressure derivative and nongradient mechanical heat production terms in the energy equation [Eq. (13) of Ref. 5] are negligible (i.e., nonhypersonic flow).
6) The flow is quasisteady ($\partial\bar{\partial}/\partial t = 0$), and two-dimensional ($\partial\bar{\partial}/\partial z = 0 = \bar{w}$) in the plane of Fig. 1. The port half-height δ is taken to be constant.
7) The flow is of thin shear-layer type, viz., $\partial\bar{\partial}/\partial y \gg \partial\bar{\partial}/\partial x$ with $\partial\bar{p}/\partial y = 0$, and is symmetric about $y = \delta$ in the mean.

Analysis

The analysis closely follows that of Ref. 5, with the exception that boundary conditions appropriate for flow in a two-dimensional (i.e., planar) grain port and a surface roughness model will be implemented. The two-dimensional geometry (Fig. 1) approximates the configurations experimentally investigated by Yamada et al. for cold flow simulations, and by Stokes et al.[10] for erosive burning. The port half-height δ (distance from surface to centerline) will be assumed constant in the present investigation.

Enthalpy and Mass Fraction Similarity

Major assumptions are summarized in Table 1. Upon invoking assumptions 1-3, and as a consequence of assumption 5, it has been shown[5] that the general unsteady gas phase equations for species mass fraction (Y_α, $\alpha = 1 \ldots N$) and total (sensible plus kinetic) enthalpy H may be reduced to a single equation for a variable f, i.e.,

$$(\rho f)_{,t} + (\rho u^\ell f)_{,\ell} = g^{\ell m}(\mu f_{,m})_{,\ell} + \omega$$

where

$$f = (\Delta h_g)^{-1}(H - H_e + \Delta h_g) = (Y_\alpha - Y_{\alpha *})/(Y_{\alpha e} - Y_{\alpha *})$$

$$\Delta h_g = \sum_\alpha (Y_{\alpha *} - Y_{\alpha e}) h_\alpha^0$$

and ω is the normalized chemical production term. In the above equations, Δh_g is the heat of reaction per unit mass, and the subscripts $*$ and e refer to conditions at the initial and end (equilibrium) states of reaction, respectively. The parameter ϕ appearing in the earlier analysis has here been absorbed into the definition of ω. It may be noted that the reaction is not required to be completed within the considered flow region, as might occur for an extremely small "motor" or a very slow reaction.

For complete similarity to exit, the boundary conditions for mass fractions and enthalpy must be identical when expressed in terms of the variable f. If the motor head end is assumed nonreactive and adiabatic, then equilibrium exists so that $f = 1$ there. Assumption 7 precludes the influence of an arbitrary downstream boundary condition on f. Hence, the behavior of thermodynamic variables (excluding pressure) within the port will be affected primarily by boundary conditions at the propellant surface. The surface boundary conditions for Y_α and H can be written for a port of rather general cross-sectional shape as[5]

$$f_s = (\dot{m}_s)^{-1} \mu n^j f_{,j}\,|_s$$

where $\dot{m}_s$ is the surface mass transfer and n^j is the contravariant unit surface normal vector. As the unsteady differential equation and boundary conditions involve f alone, similarity is obtained between both mean and unsteady (turbulent) parts of Y_α and H is the gas phase.

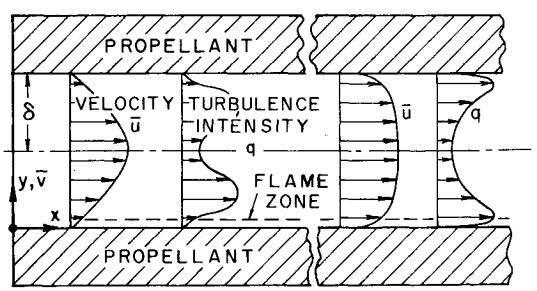

Fig. 1 Schematic representation of grain port velocity and turbulence intensity development.

The instantaneous reaction source term appearing in the f equation may be written as

$$\omega = B_g T^{\beta g} \exp(-T_{Ag}/T)\left[\frac{\rho(H_e - H)}{\Delta h_g}\right]^{\Phi}$$

An effort has been made to improve the turbulent combustion modeling used in Ref. 5 (i.e., modeling the time average, $\bar{\omega}$, and correlations involving ω'). Specifically, a second-order Taylor expansion of ω has been used to provide $\bar{\omega}$ in terms of $\bar{T}$ and $\overline{T'^2}$, and ω' in terms of T'. The resulting correlations are determined in the final equation system without the additional empiricism often associated with turbulent combustion models. The proposed model is therefore similar to models developed by Borghi[11] and others. An analytically based combustion model is favored for this problem since temperature fluctuations in the combustion region are expected to be relatively small. In preliminary calculations, however, the proposed combustion model proved to be unstable. The instability is believed due to the strict numerical coupling required by the solid-propellant problem. Consequently, the results to be presented assume $\bar{\omega} = \omega(\bar{T})$ and do not indicate the possibly important effects of turbulence on reaction rate.†

Final Equations

With Y_α expressed in terms of $H = h + u_i u_i/2$ and $h = c_p T$, use of the second-order turbulence modeling procedure of Sullivan[13] provides differential equations which, after time averaging and in boundary-layer form, are identical to those used in Ref. 5. The empirical turbulence modeling parameters (listed in the Appendix) are also identical to the values used in Ref. 5 and in the evaluation of Sullivan's procedure by Rubesin et al.[14] Overall, the complete system consists of the equations of state and continuity, and parabolic differential equations for $u, h, \overline{u'u'}, \overline{u'v'}, \overline{v'v'}, \overline{w'w'}, \overline{\rho'u'}, \overline{\rho'v'}, \overline{h'u'}, \overline{h'v'}$, and $\overline{h'h'}$. The second-order correlation equations are quite lengthy and are not listed here. They correspond with the correlation equations of Sullivan, but with the terms $\Delta h_g \overline{\chi'\omega'}$ (where χ' represents u', v', $2h'$) appearing on the right-hand sides of the $\overline{h'u'}$, $\overline{h'v'}$, and $\overline{h'h'}$ equations. The mean equations for conservation of mass, momentum, enthalpy, and the equation of state are

$$(\bar{\rho}\bar{u})_{,x} + (\bar{\rho}\bar{v} + \overline{\rho'v'})_{,y} = 0 \tag{1}$$

$$\bar{\rho}\bar{u}\bar{u}_{,x} + (\bar{\rho}\bar{v} + \overline{\rho'v'})\bar{u}_{,y} + (\bar{\rho}\overline{u'v'})_{,y} = -\bar{p}_{,x} + (\bar{\mu}\bar{u}_{,y})_{,y} \tag{2}$$

$$\bar{\rho}\bar{u}\bar{h}_{,x} + (\bar{\rho}\bar{v} + \overline{\rho'v'})\bar{h}_{,y} + (\bar{\rho}\overline{h'v'})_{,y} = \bar{u}\bar{p}_{,x} + \bar{\mu}\left[(\bar{u}_{,y})^2 + \frac{q^2}{\Lambda^2}\left(a + b\frac{\rho q \Lambda}{\mu}\right)\right] + (\bar{\mu}\bar{h}_{,y})_{,y} + \Delta h_g \omega \tag{3}$$

$$\bar{p} = R\bar{\rho}\bar{T}\left[\sum_\alpha \bar{G}_\alpha (1 - \overline{T'T'}/\bar{T}^2) - \sum_\alpha \overline{G'_\alpha T'}/\bar{T} - \sum_\alpha \sum_\beta (\overline{G'_\alpha G'_\beta}) \Big/ \sum_\alpha \bar{G}_\alpha\right] \tag{4}$$

where $G_\alpha = Y_\alpha / W_\alpha$, a and b are turbulence modeling parameters, and Λ is the turbulent macrolength scale.

Initial and Boundary Conditions

The parabolic form of the differential equations requires initial conditions for the dependent variables to be established downstream of the head end. Experimental and analytical results[7,8] suggest that an assumed initial station of $x_0 \gtrsim 5\delta$ is more than adequately far downstream to satisfy the thin shear-layer assumption. The head-end pressure $\bar{p}_h$ is specified, and the mean static pressure at x_0 is obtained from inviscid theory. The analytical velocity profile[8]

$$\frac{\bar{u}}{\bar{u}_c} = \sin\frac{\pi}{2}\frac{y}{\delta} \tag{5}$$

is used at x_0 for both cold flow and erosive burning calculations. Velocity-scaled experimental profiles of turbulence intensity are used to satisfy initial conditions for the Reynolds stress variables, $\overline{u_i'u_j'}$. For reacting flows, the mean temperature profile is obtained from numerical solution of the energy equation for normal deflagration, and all thermal correlations are assumed null at x_0. Some sensitivity to the initial conditions is obtained in the downstream calculations for particular configurations. This sensitivity is discussed in the next section.

Boundary conditions at the propellant surface ($y = 0$) are: $u = 0$, $\bar{\rho}\bar{v} = \dot{m}_s \equiv \dot{r}\rho_\pi$, with all correlations assumed null. A linear pyrolysis relation,

$$\dot{m}_s = A_\pi T^{\beta\pi} \exp(-T_{A\pi}/\bar{T})$$

is used in conjunction with the interface condition

$$\dot{m}_s = [L_s^0 + \bar{h} - c_\pi T_i]^{-1} \bar{k}\frac{\partial \bar{T}}{\partial y}$$

to determine $\dot{m}_s$ and $\bar{T}_s$. For cold flow calculations, the parameter $\bar{v}_s$ is specified.

The geometric symmetry of the problem is utilized at $y = \delta$. The condition of symmetry implies that there must be no mean fluxes (convective, diffusive, or turbulent) through $y = \delta$. Hence, at $y = \delta$: $\bar{v} = \overline{u'v'} = \overline{h'v'} = \overline{\rho'v'} = 0$, with the normal gradients of all other dependent variables being null.

Pressure Gradient

As opposed to unconfined flows, wherein the pressure $\bar{p}$ and pressure gradient, $\partial\bar{p}/\partial x$, are imposed on the boundary layer, the pressure gradient for confined boundary-layer flows evolves as part of the solution. The value of $\partial\bar{p}/\partial x$ must be consistent with the condition of conservation of mass ($\bar{v}_c = 0$) in the port. Utilizing this condition and the condition $\partial\bar{p}/\partial y = 0$, the momentum equation (2) may be integrated to yield

$$\frac{d\bar{p}}{dx} = \frac{-1}{\delta}\left[\bar{\mu}\frac{\partial \bar{u}}{\partial y}\Big|_s + \frac{d}{dx}\int_0^\delta \bar{\rho}\bar{u}^2 dy\right]$$

The first term within the brackets represents the decrease in static pressure due to surface shear, and the second term contains the effects of mass addition and change of momentum profile shape on static pressure. The latter effect

†A reviewer has justifyably questioned the realism of results obtained without accounting for the effects of turbulence on reaction rate (combustion-turbulence interaction). Further research on this topic has been performed since the original manuscript was submitted, and will be presented in detail in a subsequent paper. Insofar as the present results are concerned, it has been found that combustion-turbulence interaction can affect the mean reaction rate and turbulent diffusivity profiles. However, the collective effects on the mean temperature profile and on erosive burning are, surprisingly, quite small. These results qualitatively agree with the recent findings of Borghi and Dutoya,[12] who used an empirically specified PDF to model interaction effects for an entirely gas phase problem.

is excluded from typical one-dimensional grain port flow calculations.

Surface Roughness Model

In Ref. 15, a preliminary model for small surface roughness has been developed which is compatible with the second-order closure technique and allows direct integration to the mean surface. The model is based on the concept of Rotta (in Ref. 16) that the turbulent macrolength scale at the surface, Λ_s, tends to a nonzero value which is characteristic of the physical roughness height. It has been shown in Ref. 15 that the empirical relation $\Lambda_s = k_s/6.5$ (where k_s is the equivalent sand roughness height) satisfactorily correlates flat-plate experimental data for buffer and logarithmic region velocity profiles, and for surface friction. For "fully rough" surfaces[16] the model becomes invalid, but this condition was not exceeded in the present calculations.

It will be shown that the calculations for erosive burning are quite sensitive to the value of surface roughness assumed. However, there are difficulties in implementing this—or any roughness model—for propellant surfaces. One problem is that the standard measure of surface roughness (equivalent sand roughness) is difficult to estimate for "typical" propellant surfaces undergoing combustion. Another aspect to consider is that the actual peak-to-valley roughness height can depend upon pressure. Caveny[17] indicates that for composite propellants, for example, the roughness height may scale as a function of the absolute difference between oxidizer and average propellant burning rate, and hence would change from head to nozzle end along the grain. In the present work, these additional complexities are neglected by utilizing constant values of k_s equal to estimated peak-to-valley propellant roughness heights.

Results and Discussion

Grain Port Cold Flow Simulations

The cold flow simulations of Dunlap and Yamada have shown that, based on values of surface transpiration Reynolds number ($Re_s \equiv \bar{\rho}_s \bar{v}_s \delta / \bar{\mu}_s$) which are typical of real motors (order 10^3), the mean longitudinal velocity profile in the port corresponds with self-similar solutions for *inviscid*, laminar flow. Yet, both experiments have also indicated that turbulence intensity profiles increase in magnitude, and that the height of maximum intensity moves closer to the port surface with increasing distance from the head end. This nonsimilar behavior of turbulence and velocity provides a critical test of grain port hydrodynamic modeling.

Mean Velocity Profiles

A comparison of present (SPEC) model predictions with the velocity profile data of Yamada is shown in Fig. 2 for $x = 25$ cm. The agreement between prediction, experimental data, and the inviscid theoretical description given by Eq. (5) is quite good. Similar agreement is also obtained at the $x = 15$, 20, and 29 cm experimental stations (not shown). If allowance is made at the initial station for the fact that the calculations assume $\bar{v}_s = 1.2$ m/s, whereas $\bar{v}_s$ changes somewhat along the experimental surface (its bulk average is 1.2 m/s), then good agreement is also obtained with the unnormalized velocity profiles shown in Fig. 2 of Ref. 8. Agreement between calculations and inviscid theory is expected when both viscous and Reynolds stresses are negligible in Eq. (2). In this case Eq. (5) is an approximate solution for incompressible flow.

In a computational experiment, it is a simple matter to "lengthen" the port. This has been done to investigate whether the inviscid profile persists at higher center port Reynolds numbers, $Re_c \equiv \bar{\rho}_c \bar{u}_c \delta / \bar{\mu}_c$, than those obtained in the 29 cm length channel of Yamada, et al. Contrary to the conclusions of Yamada et al., the present model predicts (Fig. 2) a transition from a laminar to a turbulent velocity profile,

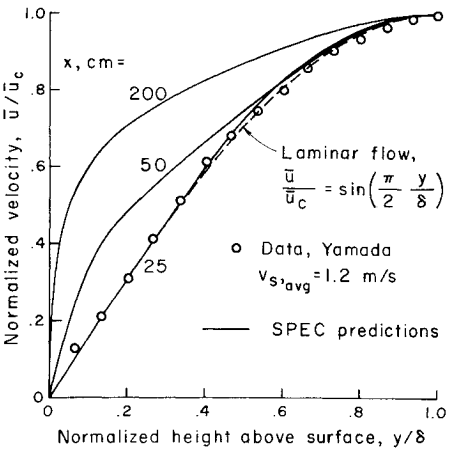

Fig. 2 Velocity profiles in cold flow simulation of two-dimensional grain port.

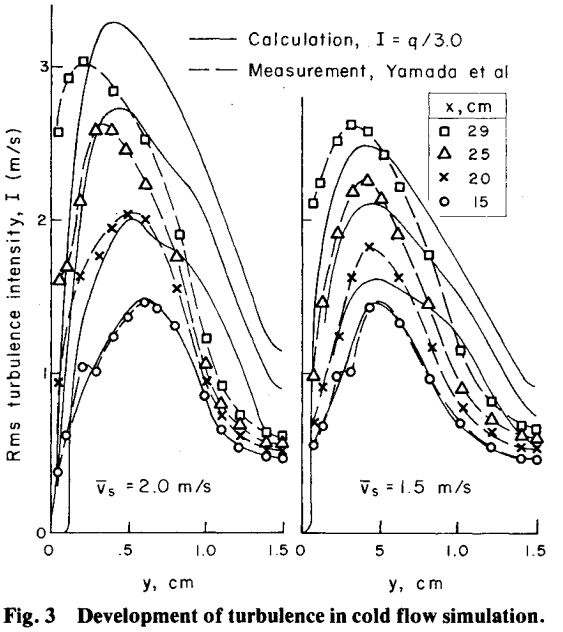

Fig. 3 Development of turbulence in cold flow simulation.

beginning at about 50 cm. The profiles continue to develop in steepness of surface gradient, such that by $x = 200$ (Mach number ≈ 0.6), the velocity profile is nearly represented by a 1/7 power law. The mechanism of transition will be discussed subsequently.

Behavior of Turbulence Intensity

A comparison between the intensity profile data of Yamada et al. and the model calculations is shown in Fig. 3 for two values of $\bar{v}_s$. For these calculations $x_0 = 15$ cm has been chosen to correspond with the first downstream profile, and $k_s = 65$ μm is assumed to characterize the surface roughness. Qualitatively, the calculations show behavior similar to data in that turbulence increases in magnitude, with the height at which maximum intensity occurs (y_m) decreasing as x increases. Quantitatively, however, it was found necessary to multiply the intensity data (denoted by the symbol I) by a factor of 3.0 at the initial station to achieve downstream growth rates in calculated turbulence intensity (q) similar to the experimental values shown. This would appear to imply a quantitative deficiency in the modeling of turbulence development for the specific configuration. However, the calculated maximum intensities (here denoted by q_m) obtained from Fig. 3 are in the range of 12-15% of $\bar{u}_c$. These values are consistent with the relative intensities found in the Dunlap investigation and also in Fig. 5 of Ref. 8.

In addition to the sensitivity of the calculations to the magnitude of the turbulence initial conditions, some sensitivity to the assumed value of k_s is also observed. This sensitivity is reflected in the growth rates of the turbulent fluctuations, and in the initiation of the mean velocity profile transition process. It has also been found that the laminarization effect of the large, favorable pressure gradient exerts a strong influence on turbulence in the initial region of the flow. This leads to the question of how initial (preturbulent) disturbances are generated in the head-end region of the port. Possible mechanisms include the direct generation of vortical disturbances by the porous surface or air supply system, and the presence of acoustic disturbances which have propagated upstream in the flow. Neither of these effects has been included in the present analysis.

Notwithstanding the laminarizing effects due to large favorable pressure gradients (which diminish with axial distance in the port), an argument is now presented on why transition within a port is possible and often probable. Consider the scaling of terms in the momentum equation (2) for incompressible flow. The convective and pressure gradient terms may be scaled to within multiplicative constants as[7,8]

$$\frac{D\tilde{u}}{Dt} \sim \frac{-d\tilde{p}/\rho}{dx} \sim x$$

As an approximation, the Reynolds stress term, $\partial\overline{u'v'}/\partial y$, will scale as $I_m^2/y_m\,(\sim q_m^2/y_m)$. Both calculations and data indicate that in most cases, I_m^2/y_m grows faster than x. For example, if the data correlations of Ref. 8 are used, $I_m^2/y_m \sim \tilde{u}_c^{1.6}\exp(-1/\tilde{u}_c)$, which for large $\tilde{u}_c \sim x^{1.6}$. Hence, given a port of sufficient length, transition should occur unless a sonic condition occurs first. Accurate prediction of the transition region will depend on the adequacy of turbulence modeling and knowledge of initial conditions. Confirmation of the transitional behavior of the velocity profile may be found in the porous tube measurements of Olson.[18] These results were, however, obtained at surface transpiration Reynolds numbers lower than those associated with typical solid-propellant motors.

Reacting Flow and Erosive Burning

In the experiment of Stokes et al.,[10] a "slab" motor (approximating the two-dimensional conditions of Fig. 1) was used to generate appreciable erosive burning. Assuming that the mean flow and turbulence can attain quasisteady conditions within the 0.06 s test times, and neglecting the ≈15% variation of δ, a simulation of two-dimensional flow within the port can be obtained with the SPEC model. Greater reservations exist concerning simulation of the composite propellants used in Ref. 10 with the present homogeneous combustion model. However, the explicit appearance of a combustion model does not occur in many erosion theories. Additionally, it has been well established that a key parameter affecting erosive burning is the normal burning rate $\dot{r}_n$. The SPEC model is able to represent aerochemically (over a limited range of interest) the normal burning rate pressure dependence of the EBT propellant used in Ref. 10, viz., $\dot{r}_n = 0.92\,(p/p^*)^{0.55}$ cm/s. The parameters used to obtain this correlation are listed in Table 2, and have been estimated from Refs. 5 and 10.

Table 2 Thermochemical parameters

$T_e = 2976$ K (adiabatic flame temperature)
$c_p = 1.92\times10^{-3}$ J/kg − K
$W_\alpha = W_{av} = 25.8$ g/g-mole
$T_{Ag} = 2.0\times10^4$ K
$B_g = 1.59\times10^{10}\,g^{1-\Phi}\,cm^{\Phi-1}\,s^{-1}\,K^{-\beta g}$
$\Phi = 1.10$
$\beta_g = 0$
$\mu = 4.42\times10^{-6}\,T^{0.65}$ poise
$T_i = 300$ K
$L_s^0 = 8.37\times10^{-2}$ J/kg
$\rho_\pi = 1.70$ g/cm^3
$c_\pi = 1.46\times10^{-3}$ J/kg − K
$\beta_\pi = 0$
$A_\pi = 2.50\times10^6$ g/cm^2-s
$T_{A\pi} = 1.0\times10^4$ K

Erosive Burning and Effect of Surface Roughness

Using the formulated initial and boundary conditions, and the physical parameters of Table 2, a comparison of SPEC model results with the experimental data of Stokes et al. is shown in Fig. 4. Comparison is made for two values of head-end pressure $\bar{p}_h$. Both the data and the one-dimensional, frictionless, nonerosive pressure calculations adapted from Ref. 10 have been corrected (by ≈3%) at the head end to correspond with the tabulated values,[10] viz., $\bar{p}_h = 79.5$ and 60.0×10^7 dyne/cm^2 for tests EBT-3 and EBT-4, respectively. The corresponding values of δ (0.415, 0.404 cm) used in the calculations are obtained from the initial value plus the distance burned measurements at the head end. Initial conditions are specified at $x_0 \approx 9\delta$.

Considering the lower pressure EBT-4 results first, increasing the surface roughness height k_s produces increased [illegible]on and hence decreased pressure along the port. For $k_s = 0$, slight erosion is obtained, such that the regression ratio $\dot{r}/\dot{r}_n$ is only 1.07 at $x \approx 50$. Prior results[5] of the SPEC model for smooth surfaces and unconfined boundary layers yielded underprediction of typical data by factors of two or three for lower burning rate propellants. Although this was attributed to the assumed combustion mechanism in Ref. 5, it is possible that the effects of surface roughness and combustion model are of equal importance for the quantitative prediction of erosion. One effect of surface roughness is to decrease the viscous sublayer height, thus increasing ambient turbulence levels in the flame zone. This effect can, in principle, compensate for some inadequacies of the combustion model (e.g., a lower than actual flame height). However, the value of k_s which produces the best agreement with the EBT-4 data is 46

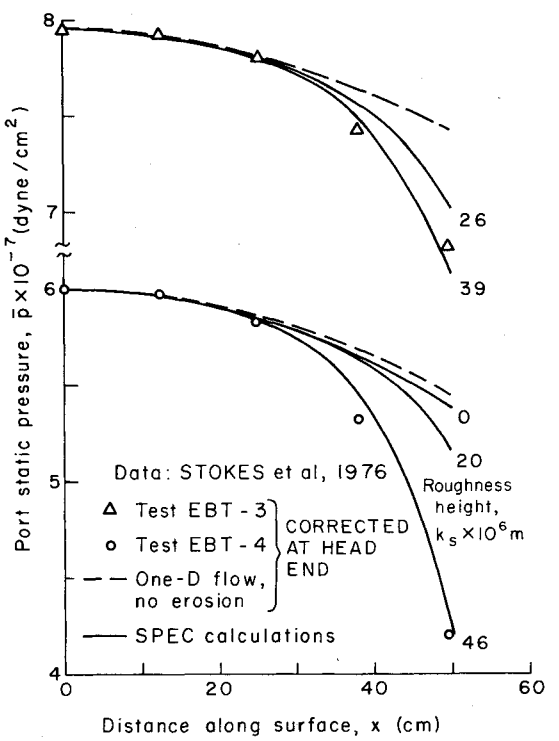

Fig. 4 Effect of surface roughness height k_s on port static pressure development with erosive burning.

μm. This value is approximately 10% of the large (400 μm) ammonium perchlorate crystal size used in the EBT formulation, and is not believed inordinate. Values of surface roughness in the 30-100 μm range (for both composite and homogeneous propellants) have been used in the erosive burning analysis of Mukunda.[3]

Maintaining all other conditions constant, the head-end pressure is increased from the EBT-4 to the EBT-3 test value in the top of Fig. 4. In this case a value of $k_s = 39$ μm provides the best agreement with data, a slight decrease from the EBT-4 results. The decrease is probably within the range of experimental error, although the possible effect of pressure on surface roughness noted previously in the paper may be present. (The burning rates of EBT and pure AP are more equivalent at this pressure.)

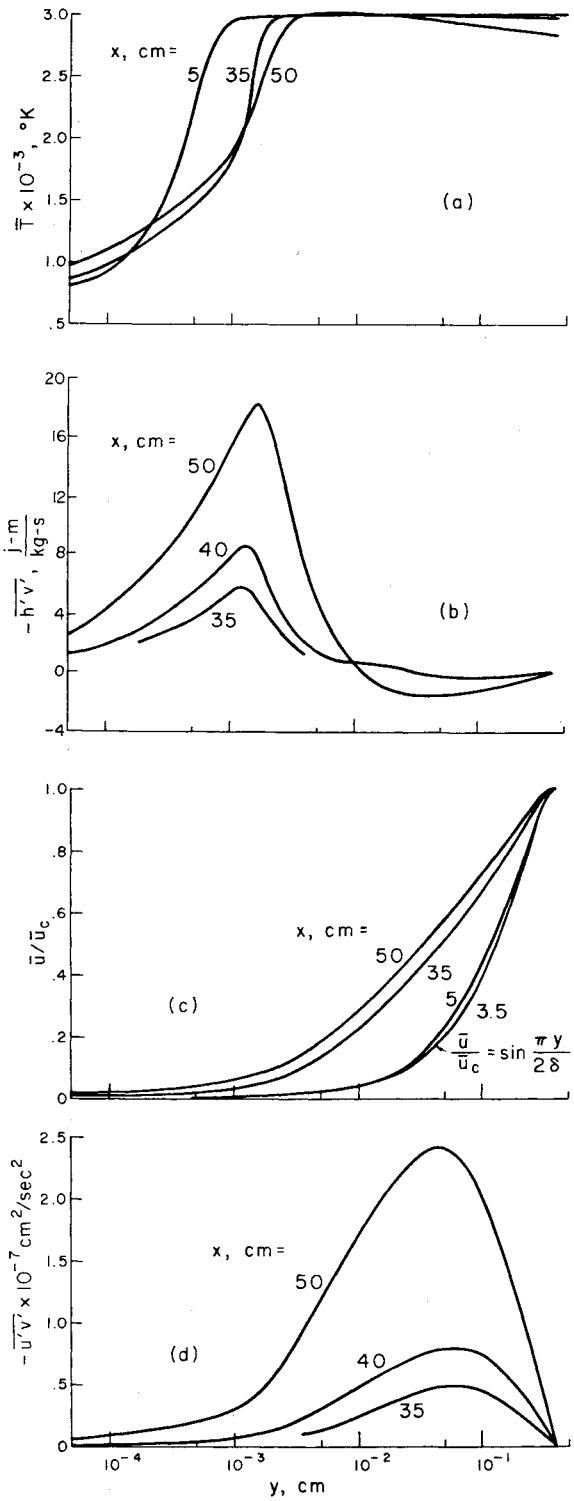

Fig. 5 Profile development in two-dimensional grain port: a) mean temperature; b) turbulent heat transfer correlation; c) normalized mean velocity; d) turbulent shear stress correlation, EBT-4 conditions, $k_s = 46$ μm.

Profile Development in Grain Port

Figure 5 shows the predicted development of key dependent variables within the slab-motor port. Computational conditions correspond to the EBT-4 run in Fig. 4 with $k_s = 46$ μm. Elements of the basic interaction mechanisms between mean and turbulent variables have been discussed in Ref. 5. Qualitative differences between the present and prior results will be discussed herein.

The temperature profile at $x = 5$ cm in Fig. 5a is identical to the normal (strand) burning profile. It persists (being scaled in height by change in pressure) until the start of erosive burning at $x = 20$. By $x = 35$, the propellant regression ratio $\dot{r}/\dot{r}_n$ has reached 1.9, which is reflected by the change in temperature gradient near the surface. Considering the rapidly changing pressure, the temperature profile at $x = 50$ ($\dot{r}/\dot{r}_n \approx 3.5$) reflects severe diffusive broadening due to turbulence. The temperature profile in the main portion of the port is decreased somewhat due to adiabatic acceleration (Mach number = 0.69 at $x = 50$), but this does not perceptibly affect the flame zone.

The turbulent contribution to heat flux may be written as $\rho\overline{h'v'}$ to second order. Figure 5b shows that $\overline{h'v'}$ is correlated with flame position and temperature gradient. This suggests that a diffusive approximation of turbulent heat flux may be valid for alternative erosive burning analyses.

Normalized velocity profiles are shown in Fig. 5c. Utilizing Eq. (5) as an initial condition at $x_0 = 3.5$, the velocity profile shows signs of a transitional "bulge" in the lower portion of the boundary layer at $x = 5$. By $x = 35$, transition has been completed and erosion is severe. In this and other calculations to be presented for this propellant, erosive burning consistently occurs subsequent to transition. Apparently, it is the large increase in surface velocity gradient which enables the production of sufficient turbulence (Fig. 5d) to enter the flame zone (Fig. 5a).

It is also noted that the calculations shown in Fig. 5 are much less sensitive to the initial conditions placed on the Reynolds stresses than are the cold flow calculations previously discussed. The precise reason for this has not been determined, but may well be related to the gas-phase density change induced by combustion.

Effect of Port Size on Erosive Burning

Mihlfeith[19] has observed that the widely used Lenoir-Robillard (L-R) theory,[20] as well as some other theories, are deficient in their ability to scale erosive burning as a function of port size. Specifically, it was noted that the L-R theory overpredicts erosive burning in full-scale motors when initially correlated with subscale data. A comparison of the present theory with that of Lenoir and Robillard is therefore warranted, with particular interest in the geometric scaling of erosive burning. Stokes et al. have correlated the L-R theory to the experimental static pressure results shown in Fig. 4. In the present notation, the L-R expression for regression rate may be written as[10]

$$\dot{r}_{LR} = \dot{r}_n + \alpha_L (\bar{\rho}_c \bar{u}_c)^{0.8} (2\delta)^{-0.2} \exp(-\beta_L \dot{r}_{LR} \rho_s / \bar{\rho}_c \bar{u}_c)$$

The parameters $\alpha_L = 0.0245$ and $\beta_L = 42$ were evaluated[10] using a least-squares procedure. Theoretical comparisons have been made by utilizing SPEC-calculated values of $\bar{\rho}_c$ and $\bar{u}_c$ along the port.

Results of the comparison are shown in Fig. 6. The regression ratios for increasing values of δ have been plotted as a function of centerline mass flux, $\bar{\rho}_c \bar{u}_c$. Considering the

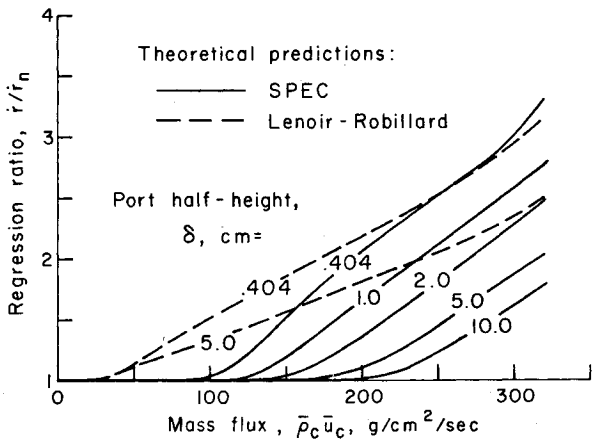

Fig. 6 Effect of port size on erosive burning as function of centerline mass flux, $k_s = 46\ \mu$m.

$\delta = 0.404$ case, both theories show similar regression ratios at higher values of mass flux, this being required to produce the experimental static pressure results of Fig. 4. At lower values of mass flux, the L-R theory predicts greater erosion. This is partly due to the use of centerline rather than bulk average velocities in the expression for $\dot{r}_{LR}$. The centerline velocities become within 20% of bulk velocities subsequent to transition, i.e., at mass velocities where the SPEC model shows erosion.

As the port half-height δ is increased, SPEC calculations (denoted by solid lines) show a continuous decrease in regression ratio at constant mass flux. For the given motor, most of the decrease in regression ratio is attributed to a translational increase in threshold mass flux. Although there is a slight decrease in slope for large δ, SPEC-calculated regression ratios appear to scale with the shift in threshold mass velocity. By comparing the L-R and SPEC calculations for $\delta = 5$ cm, the SPEC model is shown to predict less erosion with geometric scale-up. Qualitatively, this behavior in the L-R model is largely due to the lack of threshold velocity dependence upon scale. Similar results are obtained for other values of δ.

Conclusions

The major conclusions of this research may be summarized as follows.

1) The SPEC model has been compared with experimental data in cold flow simulations of a two-dimensional grain port. These comparisons show good agreement with laminar theoretical description for mean velocity profile in the Reynolds number range of data.

2) At higher center port Reynolds numbers, transition to a turbulent velocity profile is predicted to occur. This prediction contradicts the conclusions of recent experimental investigations, i.e., the inviscid velocity profile does not necessarily persist throughout laboratory or full-scale motors. The plausibility of transitional behavior is justified with an argument based on the development of turbulence within the port.

3) The completion of transition is followed by the start of erosive burning in theoretical comparisons with laboratory motor data. The intimate connection between transition and erosive burning warrants further experimental investigation with cold flow apparatus.

4) The effects of surface roughness on erosive burning are indicated to be quite important. Although possibly compensating for some inadequacies in combustion modeling, realistic values of roughness have provided good agreement with experimental static pressure data under severe erosion conditions.

5) The effect of geometric scaling on erosive burning has been theoretically investigated for a two-dimensional motor. As port half-height (hydraulic radius) is increased, the SPEC model is shown to produce less erosion than the Lenoir-Robillard model for a specific mass velocity. This observation qualitatively agrees with recent criticisms concerning geometric scaling deficiencies in the Lenoir-Robillard model.

Appendix: Turbulence Modeling Parameters

Listed below are the non-null parameters used for the second-order closure modeling of Sullivan.[13] Note that some of the parameters appear only as collective products in the final equations. The uppercase notation is consistent with the computer generated format of the equations.

$$A = 3.25$$
$$B = 0.125$$
$$CLAMB = 0.17$$
$$DIN = 0.65$$
$$AHH = 5.85$$
$$AHU = ARU = 3.25$$
$$BHH = 0.225$$
$$VUU = VUH = VHH = 0.1$$
$$VRU = VRH = VRR = 0.1$$
$$PMU2 = PMH2 = PMR2 = 1.0$$
$$PTHM = PTUM = 0.15$$
$$PGH2 = PGR2 = 0.8$$
$$PGU = PGU2 = 1.0$$
$$WWU1 = WWR1 = WWH1 = -0.1$$
$$WWGU = -0.5$$
$$WWGR = WWGH = -1.0$$

Acknowledgment

This research has been supported by the Air Force Office of Scientific Research under prime Contract F44620-78-C-0016; Capt. R. F. Sperlein, program manager. The assistance of Mr. Asad Khan of Rutgers University in performing the calculations was appreciated.

References

[1] Williams, F. A., Barrere, M., and Huang, N. C., "Fundamental Aspects of Solid Rockets," AGARDograph 116, Chaps. 4, 6, and 7, Oct. 1969, pp. 339-456.

[2] Kuo, K. K. and Razdan, M. K., "Review of Erosive Burning of Solid Propellants," *Proceedings of 12th JANNAF Combustion Meeting*, Aug. 1975, pp. 323-338.

[3] Mukunda, H. S., "A Comprehensive Theory of Erosive Burning in Solid Rocket Propellants," *Combustion Science and Technology*, Vol. 18, 1978, pp. 105-118.

[4] King, M., "A Model of the Erosive Burning of Composite Propellants," *Journal of Spacecraft and Rockets*, Vol. 15, May-June 1978, pp. 139-146.

[5] Beddini, R. A., "A Reacting Turbulent Boundary Layer Approach to Solid Propellant Erosive Burning," *AIAA Journal*, Vol. 16, Sept. 1978, pp. 898-905.

[6] Razdan, M. K. and Kuo, K. K., "Erosive Burning Study of Composite Solid Propellants by Turbulent Boundary-Layer Approach," *AIAA Journal*, Vol. 17, Nov. 1979, pp. 1225-1233.

[7] Dunlap, R., Willoughby, P. G., and Hermsen, R. W., "Flowfield in the Combustion Chamber of a Solid Propellant Rocket Motor," *AIAA Journal*, Vol. 12, Oct. 1974, pp. 1440-1442.

[8] Yamada, K., Goto, M., and Ishikawa, N., "Simulative Study on the Erosive Burning of Solid Rocket Motors," *AIAA Journal*, Vol. 14, Sept. 1976, pp. 1170-1177.

[9] Culick, F.E.C., "Rotational Axisymmetric Mean Flow and Damping of Acoustic Waves in a Solid Propellant Rocket," *AIAA Journal*, Vol. 4, Aug. 1966, pp. 1462-1464.

[10] Stokes, B. B., Hessler, R. O., and Caveny, L. H., "Erosive Burning of Nonmetalized Composite Propellants—Data Acquisition and Analysis," *Proceedings of 13th JANNAF Combustion Meeting*, CPIA Pub. 281, Vol. II, Dec. 1976, p. 437.

[11] Borghi, R., "Chemical Reaction Calculations in Turbulent Flows Applicable to a CO-containing Turbojet Plume," *Advances in Geophysics*, Vol. 18, 1974, p. 349.

[12] Borghi, R. and Dutoya, D., "On the Scales of the Fluctuations in Turbulent Combustion," *Proceedings of 17th Symposium (International) on Combustion*, The Combustion Institute, Pittsburgh, Pa., 1979, pp. 235-244.

[13] Sullivan, R. D., "GYC—A Program to Compute the Turbulent Boundary Layer on a Rotating Cone," A.R.A.P. Working Paper 76-2, Aeronautical Research Associates of Princeton, Inc., Princeton, N.J., Aug. 1976.

[14] Rubesin, M. W., Crisalli, A. J., Lanfranco, M. J., Horstman, C. C., and Acharya, M., "A Critical Evaluation of Second-Order Closure Models for Incompressible Boundary Layers with Axial Pressure Gradients," AIAA Paper 77-128, Aerospace Sciences Meeting, Jan. 1977.

[15] Beddini, R. A., "Preliminary Studies of Roughness and Free-Stream Disturbance Effects on Boundary Layer Skin Friction," A.R.A.P. Technical Memo. 77-11, Aeronautical Research Associates of Princeton, Inc., Princeton, N.J., June 1977.

[16] Hinze, J. O., *Turbulence*, 2nd ed., McGraw-Hill Book Co., New York, 1975, pp. 614-624.

[17] Caveny, L. H., personal communication, June 19, 1978.

[18] Olson, R. M., "Experimental Studies of Turbulent Flow in a Porous Circular Tube with Uniform Mass Transfer through the Tube Wall," Ph.D. Thesis, University of Minnesota, Minneapolis, July 1964; also, Huesmann, K. and Eckert, E.R.G., "Untersuchungen uber die laminare Stromung und den Umschlag zur Turbulenz in porosen Rohren mit gleichmassiger Einblasung durch die Rohrwand," *Warme-und Stoffubertragung*, Bd. 1, 1968, p. S2.

[19] Mihlfeith, C. M., "JANNAF Erosive Burning Workshop Report," *Proceedings of 14th JANNAF Combustion Meeting*, CPIA Publication 292, Vol. I, Dec. 1977, pp. 379-392.

[20] Lenoir, J. M. and Robillard, G., "A Mathematical Method to Predict the Effects of Erosive Burning in Solid Propellant Rockets," *Proceedings of 6th Symposium (International) on Combustion*, Reinhold Publishing, Stanford, Conn., 1957, pp. 663-667.